PNAS INAUGURAL ARTICLE | APPLIED PHYSICAL SCIENCES

Self-assembled nanocomposites of high water content and load-bearing capacity

Guogao Zhang[a,1], Junsoo Kim[a,1], Sammy Hassan[a], and Zhigang Suo[a,2]

This contribution is part of the special series of Inaugural Articles by members of the National Academy of Sciences elected in 2019.

Contributed by Zhigang Suo; received March 6, 2022; accepted June 10, 2022; reviewed by Alfred Crosby, Eric Dufresne, and Jian Ping Gong

Biological tissues, such as cartilage, tendon, ligament, skin, and plant cell wall, simultaneously achieve high water content and high load-bearing capacity. The high water content enables the transport of nutrients and wastes, and the high load-bearing capacity provides structural support for the organisms. These functions are achieved through nanostructures. This biological fact has inspired synthetic mimics, but simultaneously achieving both functions has been challenging. The main difficulty is to construct nanostructures of high load-bearing capacity, characterized by multiple properties, including elastic modulus, strength, toughness, and fatigue threshold. Here we develop a process that self-assembles a nanocomposite using a hydrogel-forming polymer and a glass-forming polymer. The process separates the polymers into a hydrogel phase and a glass phase. The two phases arrest at the nanoscale and are bicontinuous. Submerged in water, the nanocomposite maintains the structure and resists further swelling. We demonstrate the process using commercial polymers, achieving high water content, as well as load-bearing capacity comparable to that of polyethylene. During the process, a rubbery stage exists, enabling us to fabricate objects of complex shapes and fine features. We conduct further experiments to discuss likely molecular origins of arrested phase separation, swell resistance, and ductility. Potential applications of the nanocomposites include artificial tissues, high-pressure filters, low-friction coatings, and solid electrolytes.

hydrogel | polymer glass | nanocomposite | self-assemble | phase separation

The stratum corneum—the outermost layer of the epidermis—has high water content (up to 40%) and high load-bearing capacity (e.g., elastic modulus 210 MPa, strength 18 MPa, and toughness 3.6 kJ·m^{-2}) (1–3). Recent decades have seen the development of synthetic materials of high water content, but few have achieved high load-bearing capacity (4–14). This difficulty is illustrated by looking at synthetic materials of high water content on the plane of elastic modulus and toughness (Fig. 1*A*). Hydrogels can be tough but are not stiff, because of their rubbery polymer networks. A composite of glass fabric and hydrogel has both high elastic modulus and toughness (15, 16), but the coarse microstructure and the method of fabrication are unsuitable for applications that require complex shapes and fine features.

This paper reports a process that self-assembles nanocomposites of high water content and high load-bearing capacity (Fig. 1*B*). Such a nanocomposite consists of a hydrogel-forming polymer and a glass-forming polymer. The process separates the polymers into a hydrogel phase and a glass phase. The two phases arrest at the nanoscale and are bicontinuous. The continuous hydrogel phase transports small molecules, and the continuous glass phase bears loads. In each phase, the two species of polymers interpenetrate. The hydrogel phase traps glass-forming polymers, and the glass phase traps hydrogel-forming polymers. We show that the hydrogel-forming polymers trapped in the glass can plasticize a brittle glass. For example, at room temperature, pure poly(methyl methacrylate) (PMMA) is a brittle glass, but a nanocomposite of PMMA and poly(acrylic acid) (PAAc) of two-to-one weight ratio is ductile. The nanocomposite has a water content 45.2%, elastic modulus 506 MPa, strength 15.5 MPa, toughness 5.8 kJ·m^{-2}, and fatigue threshold 1.85 kJ·m^{-2}. Such a combination of high water content and high load-bearing capacity has never been realized before in synthetic nanomaterials. The nanocomposites can be fabricated into objects of complex shapes and fine features. Submerged in pure water, the nanocomposites resist swelling by the yield strength of the glass phase.

PMMA–PAAc copolymers have been prepared for various applications such as drug delivery (17), tissue repair (18), bioimplant (19), and strong adhesion (20). Many of these materials have nanoscale structures and a wide range of mechanical properties. Hydrogels of PMMA–PAAc copolymers have also been reported before (18, 20), but the modulus of the hydrogels is a few kilopascals, which indicates that no continuous glassy phase is formed. By comparison, the PMMA–PAAc nanocomposite in this work

Significance

Many biological tissues are nanocomposites of high water content and load-bearing capacity. These properties are important for biological functions, but have been challenging to mimic in synthetic materials. Here we meet this challenge by developing a self-assembling process, in which two polymer phases form, interpenetrate, and arrest at the nanoscale. We demonstrate the process using widely available glass-forming and hydrogel-forming polymers. The resulting nanocomposites achieve high water content and high load-bearing capacity. Furthermore, the process enables the nanocomposite to be fabricated into objects with complex shapes and fine features. This self-assembling process opens doors to combine extremely different polymers to achieve unusual properties. The process is generally applicable for natural and synthetic polymers.

Author contributions: G.Z. designed research; G.Z., J.K., and S.H. performed research; G.Z., J.K., S.H., and Z.S. analyzed data; and G.Z., J.K., S.H., and Z.S. wrote the paper.

Reviewers: A.C., University of Massachusetts Amherst; E.D., Eidgenossische Technische Hochschule Zurich; and J.P.G., Hokkaido Daigaku.

The authors declare no competing interest.

[1]G.Z. and J.K. contributed equally to this work.

[2]To whom correspondence may be addressed. Email: suo@seas.harvard.edu.

This article contains supporting information online at http://www.pnas.org/lookup/suppl/doi:10.1073/pnas.2203962119/-/DCSupplemental.

Published July 18, 2022.

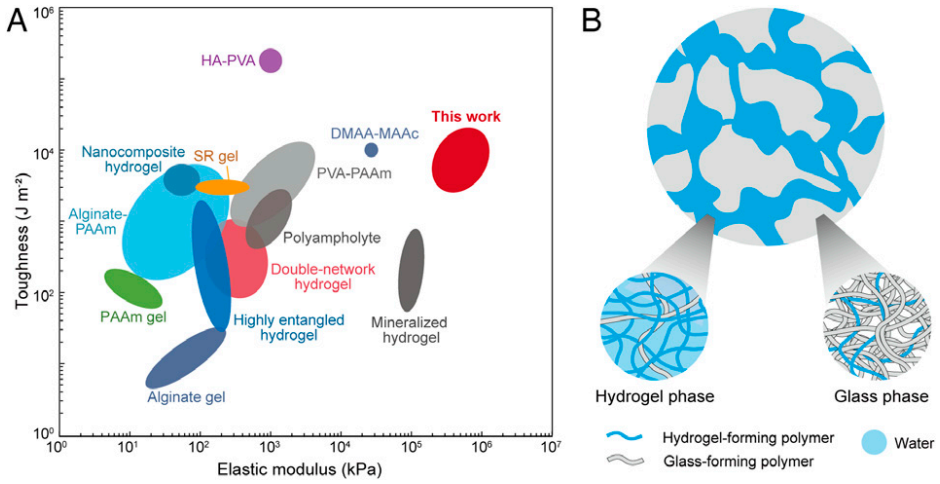

Fig. 1. Synthetic materials of high water content. (*A*) The materials synthesized in this work are compared with existing synthetic materials of high water content on the plane of elastic modulus and toughness (4–14). HA-PVA, hierarchical and anisotropic poly(vinyl alcohol); PVA, poly(vinyl alcohol); DMAA, N,N-dimethylacrylamide; MAAc, methacrylic acid; PAAm, polyacrylamide. References to the existing materials are listed in *SI Appendix*, Table S1. (*B*) A nanocomposite of a glass phase and a hydrogel phase, self-assembled by two species of polymers.

forms a continuous glassy phase and has a modulus of over 100 MPa. Moreover, the process described here starts from pre-existing polymers, and is applicable to commercially available polymers and biobased polymers.

Results and Discussion

We first demonstrate this process by synthesizing a nanocomposite of a hydrogel-forming polymer, PAAc, and a glass-forming polymer, PMMA. The PMMA used in this work all comes from commercial acrylic films, of which the main component is linear PMMA polymers. The process has four stages (Fig. 2*A*). PMMA is a linear polymer with a brittle-to-ductile transition temperature of about 80 °C (21). At room temperature, pristine PMMA is a transparent and brittle glass (stage I). We form a solution of water and acrylic acid (AAc) of molar ratio $W = 4$. The solution also contains dilute concentrations of initiator and cross-linker for the AAc monomers to polymerize and cross-link upon UV

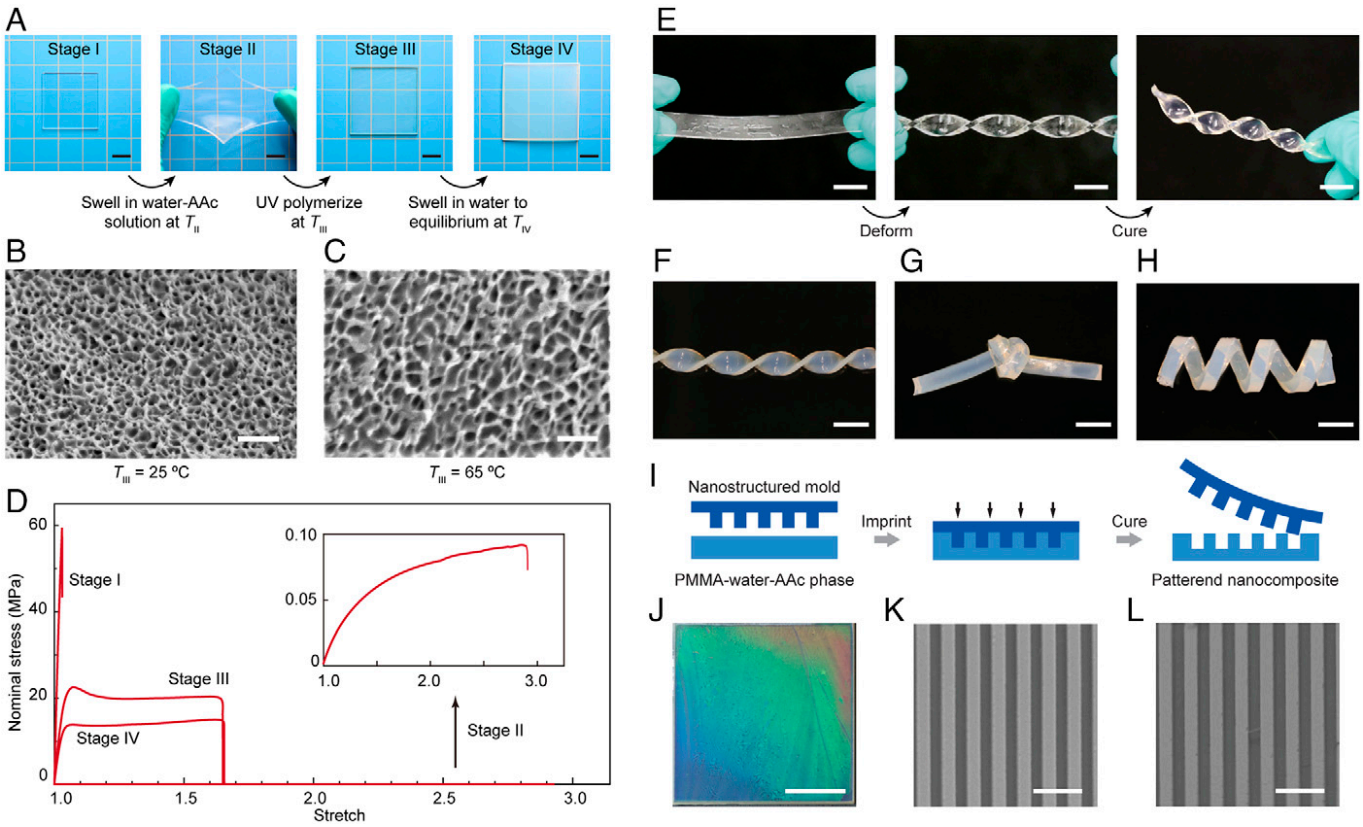

Fig. 2. Synthesis and shaping of nanocomposites. (*A*) A film in four stages during synthesis. (Scale bars, 2 cm.) (*B* and *C*) The scanning electron microscope (SEM) images of the composite in stage III prepared at two temperatures, T_{III} = 25 °C (*B*) and 65 °C (*C*). (Scale bars, 500 nm.) (*D*) The stress–stretch curves of the film in the four stages. (*E*) The film in stage II deforms readily, and maintains the deformed shape after cure in stage III. (Scale bars, 2 cm.) (*F–H*) Various shapes of the nanocomposite in stage IV. (Scale bars, 2 cm.) (*I*) A film in stage II is imprinted with a mold of a line pattern, and retains the pattern after cure in stage III. (*J*) The patterned nanocomposite iridesces. (Scale bar, 2 cm.) (*K* and *L*) The SEM image of the mold (*K*) and the patterned nanocomposite (*L*). (Scale bars, 2 μm.)

irradiation. In a dark chamber, when a thin film of PMMA is submerged into the water–AAc solution at a temperature denoted by T_{II}, AAc monomers do not polymerize, and PMMA swells, forming a single phase of the three principal components: PMMA, water, and AAc (stage II). The PMMA–water–AAc phase is transparent and rubbery, and is separated from the water–AAc solution. The phase also contains the initiator and cross-linker, but their low concentrations negligibly affect the phase behavior. The solubility of PMMA in the water–AAc solution is negligible. Under a UV lamp, the AAc monomers polymerize and cross-link, and the PMMA–water–AAc phase separates into a glass phase and a hydrogel phase, but remains transparent (stage III). Polymerization is conducted at a temperature T_{III}, which affects the sizes of the separated phases (Fig. 2*B* and *C*). The sizes of the phases are ∼90 nm at T_{III} = 25 °C and ∼180 nm at T_{III} = 65 °C. Submerged in pure water, the sample swells and becomes translucent (stage IV). The temperature at which stage IV is prepared, T_{IV}, affects polymer content but does not cause further coarsening (*SI Appendix*, Fig. S1). The microstructures are uniform across the thickness of the sample (*SI Appendix*, Fig. S2). The samples in stage III and IV will be called PMMA–water–PAAc nanocomposites. For the following studies, T_{III} is fixed at 25 °C.

The samples in various stages are compared by handling in hands (Movie S1). This comparison is made quantitative by their stress–stretch curves (Fig. 2*D*). Unless otherwise noted, all the mechanical tests are conducted within 5 min in the open air, and the mass change is less than 3%. The pristine PMMA (stage I) is a brittle glass, and the stress rises steeply, and the sample ruptures at a stretch of about 1.04 without plastic deformation. The PMMA–water–AAc phase (stage II) is a rubber, and the stress is low, and deformation is large. The PMMA–water–PAAc nanocomposite (stage III and IV) is glassy but ductile, and the stress rises steeply initially, followed by plastic flow before rupture.

In a nanocomposite, the PMMA-rich phase is a polymer glass, and the PAAc-rich phase is a polymer gel. The two phases are bicontinuous. The stress–stretch curves for the nanocomposite show high elastic modulus and high strength, which indicate that the PMMA-rich phase is continuous. To demonstrate that the PAAc-rich phase is continuous, we prepare a blue-colored solution by dissolving 0.5 wt% of Acid Violet 43 in water. The nanocomposite submerged in the solution turns blue homogeneously, but a pristine PMMA sample submerged in the solution does not turn blue (*SI Appendix*, Fig. S3).

The PMMA–water–AAc phase (stage II) is rubbery, enabling us to fabricate objects of complex shapes. For example, we fabricate three-dimensional structures from a strip of PMMA (Fig. 2*E* and Movie S2). Pristine PMMA itself is brittle, and cannot be deformed into a three-dimensional shape at room temperature. We swell the PMMA strip into a rubbery phase (stage II), deform it, and cure it in the deformed state. The resulting nanocomposite (stage III or IV) retains the shape after cure. For example, this process turns a strip of PMMA into three-dimensional shapes by twisting and knotting, as well as by wrapping around a silica rod (Fig. 2*F*–*H*, stage IV).

The sizes of the two phases in the nanocomposites are ∼90 nm, enabling us to fabricate objects of fine features. To illustrate, we pattern the surface of a nanocomposite by imprinting using a mold with periodic lines of a period 550 nm (Fig. 2*I*). The mold is made of perfluoropolyether (elastic modulus ∼10.5 MPa) (22, 23), which is much stiffer than the PMMA–water–AAc phase (stage II), so that imprint can be readily conducted. After cure, the mold can be easily peeled off, due to the low surface energy. The finely spaced periodic lines make the surface iridescent (Fig. 2*J*). Because the individual phases of the nanocomposite are smaller than the features of the mold, the structures imprinted on the nanocomposite are sharp and retain high fidelity to the features of the mold (Fig. 2*K* and *L*).

We study the physical chemistry of the self-assembly process. We begin with the PMMA–water–AAc phase (stage II). PMMA does not dissolve in water but dissolves in acrylic acid. Water and acrylic acid form binary solutions of any molar ratio, W. In a preliminary experiment, we submerge PMMA films in water–AAc solutions of various molar ratios. In a binary solution of low W, a PMMA film dissolves and forms a PMMA–water–AAc solution. In a binary solution of high W, the PMMA film swells into a PMMA–water–AAc phase, which does not dissolve in the water–AAc binary solution even after 2 mo. The transition from dissolution to phase separation takes place at a value of W between three and four. To confirm that PMMA chains dissolve negligibly in a water–AAc binary solution of high W, we evaporate water and AAc from the PMMA–water–AAc phase at 180 °C for 2 d, and find that the film recovers the initial volume and mass of the PMMA (Fig. 3*A*).

We also measure the properties of the PMMA–water–AAc phase after it equilibrates with the binary solution. The PMMA content in the PMMA–water–AAc phase increases with W of the binary solution (Fig. 3*B*). The elastic modulus of the PMMA–water–AAc phase increases with W, from 0.26 MPa at W = 4 to 190 MPa at W = 14 (Fig. 3*C*). We further characterize the PMMA–water–AAc phase prepared using a water–AAc solution of W = 4 at a temperature T_{II}. When a PMMA film is submerged in the binary solution, as time increases, the film swells, and its PMMA content decreases to a plateau. A high T_{II} shortens the time to plateau but does not change the level of the plateau (Fig. 3*D*). The PMMA–water–AAc phase has rate-dependent stress–stretch curves, with an elastic modulus of 260 kPa and a strength of 140 kPa at stretch rate 1 s^{-1}, and an elastic modulus of 220 kPa and a strength of 90 kPa at stretch rate 0.01 s^{-1} (Fig. 3*E*). When a PMMA–water–AAc phase is suddenly stretched to twice its original length, the stress relaxes with time to a plateau (Fig. 3*F*). The samples used in Fig. 3*E* and *F* are dip coated with a layer of mineral oil to prevent the water and AAc molecules from evaporating. Similar stress relaxation behavior is also observed in a compression test for a longer time (*SI Appendix*, Fig. S4). In subsequent studies, all the films are swollen to plateau before proceeding to the next stage, and samples are prepared at T_{II} = 25 °C using water–AAc solutions of $W \geq 4$.

We next study the nanocomposites (stages III and IV). Here, the PMMA–water–AAc phase (stage II) is cured at a fixed temperature T_{III} = 25 °C, and the obtained nanocomposite (stage III) is submerged in pure water at temperature T_{IV} to swell to equilibrium (stage IV; *SI Appendix*, Fig. S5*A* and *B*). We measure the weight change of the sample from stage III to stage IV (*SI Appendix*, Table S2). The density of the dry polymer is comparable to that of water, so that the volumetric ratio is similar to the weight ratio. When the stage IV nanocomposites are stored in pure water at room temperature, they do not swell or deswell (*SI Appendix*, Fig. S5*C*). We make nanocomposites using various values of W and T_{IV}, and measure their properties (*SI Appendix*, Table S3). For nanocomposites prepared with a binary solution of a fixed W = 4, the equilibrium water content increases with T_{IV} (Fig. 4*A*).

Both stages III and IV nanocomposites rupture after extensive plastic flow (Fig. 4*B*). High T_{IV} increases the water content but decreases elastic modulus and strength. Both elastic modulus and strength are proportional to the PMMA content (Fig. 4*C* and *D*). These linear trends are in contrast to the nonlinear relations

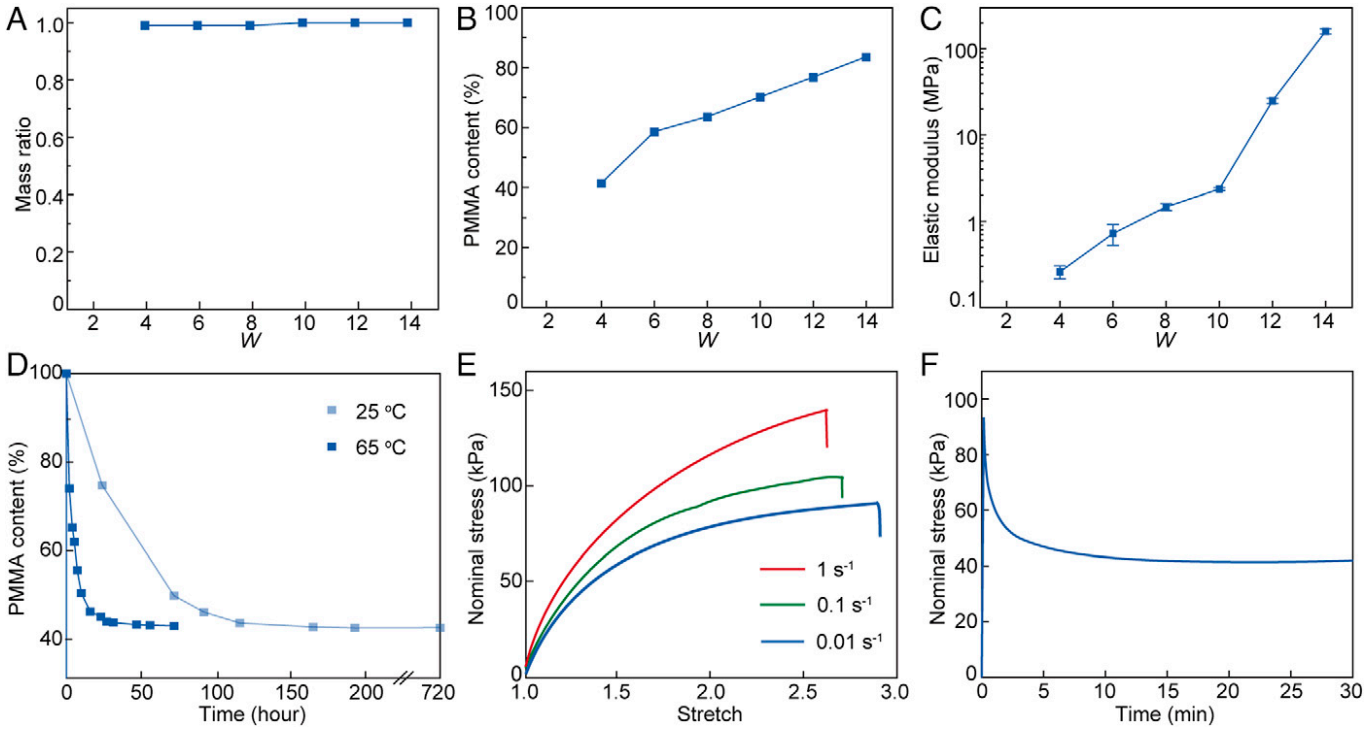

Fig. 3. Characterization of PMMA–water–AAc phase (stage II). (*A*) The mass ratio of a PMMA–water–AAc phase after the evaporation to the initial PMMA is plotted as a function of the molar ratio of the water–AAc binary solution *W*. (*B*) The PMMA content of the PMMA–water–AAc phase increases with *W*. (*C*) Elastic modulus at a stretch rate of 1 s^{-1} of the PMMA–water–AAc phase as a function of *W*. (*D–F*) PMMA–water–AAc phase prepared in a water–AAc binary solution of $W = 4$. (*D*) Submerged in the water–AAc binary solution at 25 °C and 65 °C, PMMA films of thickness 1.56 mm swell, and the PMMA contents in the films decrease to the same plateau. (*E*) Stress–stretch curves at various stretch rates. (*F*) When a sample is rapidly pulled to a constant stretch of two, the stress relaxes with time, and plateaus.

between elastic modulus and concentration commonly found in particle-filled elastomers (24, 25). The particle-filled elastomers stiffen steeply only when the particles percolate, whereas the nanocomposites here have bicontinuous nanostructures.

We measure the toughness of the nanocomposites as a function of PMMA content φ (Fig. 4*E*). When $\varphi = 58.5\%$, toughness peaks at 17.2 kJ·m^{-2}, which is much higher than that of pristine PMMA, 1.2 kJ·m^{-2}, and that of pure PAAc gel, ~100 J·m^{-2} (14). The nanocomposites readily show both high water content and excellent mechanical properties. For example, the nanocomposite prepared with $W = 4$ and $T_{IV} = 65$ °C has a water content of 45.2%, an elastic modulus of 506 MPa, a strength of 15.5 MPa, and a toughness of 5.8 kJ·m^{-2}. Next, we study the fatigue crack growth in the nanocomposite under cyclic load. To maintain the hydration level, the tests are conducted at a relative humidity of about 95%. The extension of crack per cycle d*c*/d*N* decreases with the energy release rate *G* (Fig. 4*F*). The crack does not grow when the energy release rate is below a threshold of about 1,850 J·m^{-2} (*SI Appendix*, Table S4). By comparison, PMMA has a fatigue threshold of lower than 100 J·m^{-2} (26). For the following studies, samples are prepared with $W = 4$, $T_{Iii} = 25$ °C, and $T_{IV} = 65$ °C.

We conduct further experiments to discuss likely molecular origins of several main findings. In stage III, the two phases arrest at the nanoscale. The arrest of phase coarsening in self-assembly by phase separation is an active field of research (27). Our experiments indicate that the phase coarsening is arrested by the competition between the interfacial energy and the elastic energy of the PMMA–water–AAc phase. When the stage-II PMMA–water–AAc phase is under the UV lamp, the AAc monomers polymerize and reduce the entropy of mixing, which is a principal driving force for phase separation. As AAc monomers polymerize into PAAc, the PMMA–water–AAc phase transforms into two phases, one rich in PAAc hydrogel and the other rich in PMMA glass. The growth of the new phases must be accommodated by the deformation of the surrounding PMMA–water–AAc phase. In order to understand the mechanism for the arrested phase separation more, we adopt a model of phase separation in interpenetrating networks (28). The interfacial energy drives coarsening. However, the PMMA–water–AAc phase is rubbery, and the elastic energy resists coarsening. The competition arrests coarsening at phase sizes scaled as γ/E, where γ is the interface energy and E is the elastic modulus. A representative value of interfacial energy is $\gamma = 0.016$ N·m^{-1} (29). At 25 °C and 65 °C, the moduli of the PMMA–water–AAc phase are 222 and 64 kPa (*SI Appendix*, Fig. S6), and the model predicts that the equilibrium sizes of the phases are on the order of 72 and 250 nm. These predictions approximately agree with the observed phase sizes (Fig. 2*B* and *C*). Will the yield strength s_Y of the glass phase also arrest coarsening? If it does, the phases should arrest at a size scaled as γ/s_Y. Using representative values, we predict a feature size of 0.8 nm, which is much smaller than the arrested phases observed in experiments. The glass phase, initially, is discontinuous, and the yield strength of the glass does not arrest coarsening.

When a stage III nanocomposite is submerged in pure water at temperature T_{IV}, the sample swells to equilibrium (stage IV). We propose that this equilibrium has the following molecular origin. In the nanocomposite, the swelling is mostly restricted to the gel phase, accommodated by the plastic deformation of the glass phase. In equilibrium, the residual stress in the glass phase balances the osmotic pressure in the gel phase. To see whether the driving force for swelling is large enough to cause the glass phase to undergo plastic flow, we estimate the osmotic pressure by $-kT/v[1/J + \ln(1 - 1/J) + \chi/J^2]$, where kT is the temperature in the unit of energy, v is the volume per water molecule, J is the volume of the hydrogel phase divided by the

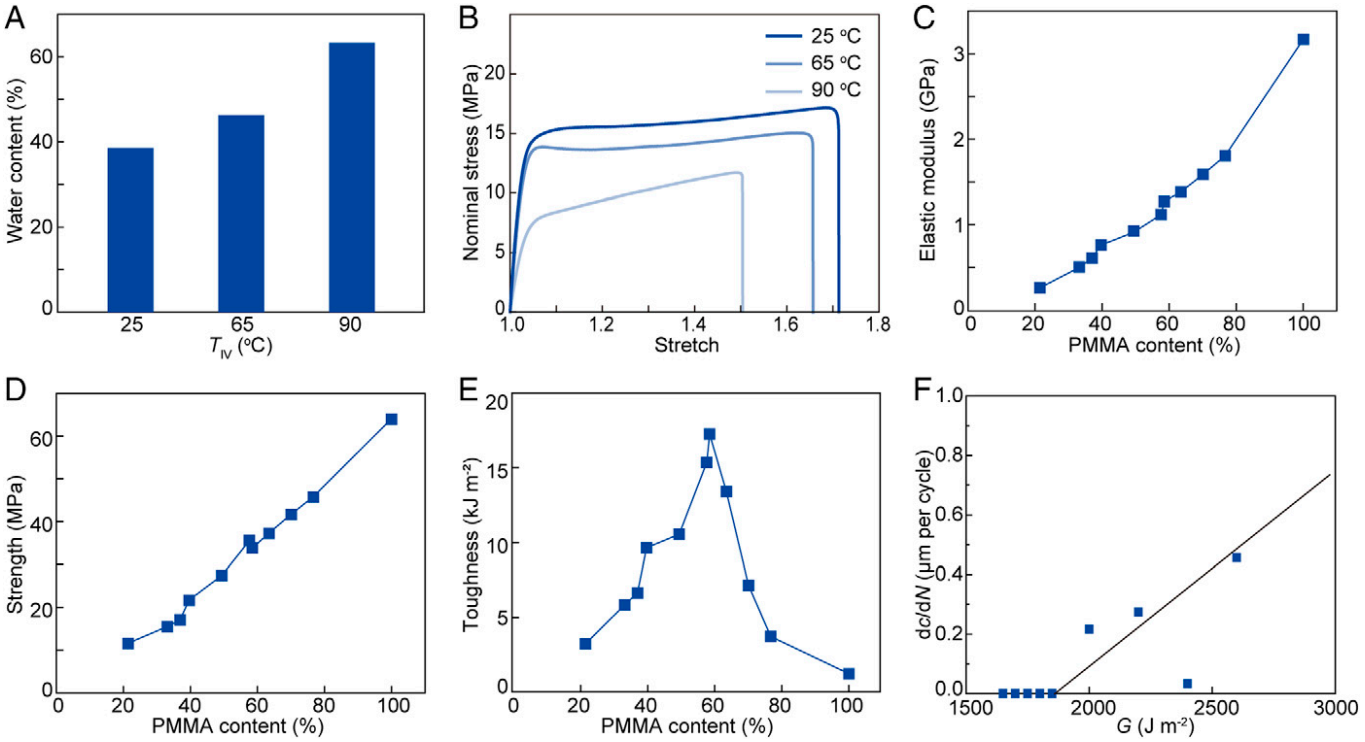

Fig. 4. Characterization of the nanocomposites (stages III and IV). (*A*) The equilibrium water contents of the nanocomposites prepared with $W = 4$ as a function of T_{IV}. (*B*) Stress–stretch curves for the nanocomposite in stage IV with the same $W = 4$ and various T_{IV}. (*C* and *D*) The elastic modulus and the strength of the nanocomposites are proportional to the PMMA content. (*E*) The toughness of the nanocomposites first increases with the PMMA content then decreases. (*F*) Fatigue crack growth in a nanocomposite prepared with $W = 4$ and $T_{IV} = 65$ °C.

volume of the PAAc, and χ is the interaction parameter of AAc and water (30, 31). For a representative value, $J \approx 2$ and $\chi \approx 0.41$ (32). The model predicts an osmotic pressure of 12 MPa, which is comparable to the yield strength of the nanocomposite (Fig. 2*D*). As temperature T_{IV} increases, the mobility of PMMA chains increases, the yield strength of the glass phase decreases, and so does the polymer content of the nanocomposite in equilibrium. After swelling in pure water to equilibrium at $T_{IV} = 65$ °C, $J \approx 3.2$, which gives osmotic pressure of ~3 MPa. The nanocomposite in this stage does not swell anymore when the osmotic pressure is less than the yield strength.

At room temperature, pristine PMMA is brittle, but a PMMA–water–PAAc nanocomposite is ductile. We propose that the ductility of the nanocomposite has the following molecular origin. In a nanocomposite, the PAAc chains are trapped in the glass phase, entangled with the PMMA chains, and associated with water molecules. Such hydrated PAAc chains plasticize PMMA-rich glass. To ascertain this picture, we submerge a stage II sample in pure water. As AAc monomers diffuse out and water molecules diffuse in, the sample separates into bicontinuous phases, PMMA and water (*SI Appendix*, Fig. S7*A*). In a tensile test, the sample ruptures without plastic flow (*SI Appendix*, Fig. S7*B*). This observation indicates that the porous structure by itself does not impart ductility to PMMA. To ascertain the importance of hydration to the ductility, we prepare a sample of stage IV, and evaporate water from the sample at 25 °C for 3 d. During the evaporation, the PAAc chains lose the water molecules. Subject to the tensile test, the dehydrated sample ruptures without plastic flow, and the sample recovers its ductility after swelling in water (*SI Appendix*, Fig. S8). These observations indicate that the hydration of the PAAc chains is important for the ductility of the nanocomposite. Interestingly, at room temperature, PMMA can absorb up to 2.2 wt% water, but the absorbed water increases ductility only slightly (33).

The method described in this paper may be contrasted by the phase inversion method (34). The phase inversion method commonly involves a thermoplastic and two liquids, A and B. The two liquids form a solution. The thermoplastic forms solution with liquid A but not with liquid B. When a concentrated solution of the thermoplastic and liquid A is submerged in pure liquid B, liquid A migrates out, and liquid B migrates in. The resulting material is a composite of thermoplastic and liquid B. By contrast, the method described in this paper involves the polymerization of AAc molecules. The polymerization drives phase separation. The resulting material consists of interpenetrating polymers. These differences can affect the sizes of arrested phases, as well as the mechanical behavior of the resulting materials. The comparison of the two methods of synthesis will depend on material systems, and will not be pursued in detail here.

Incidentally, the process that skips stage III (i.e., AAc monomers do not polymerize) is an example of the phase-inversion method. In this particular example, after AAc diffuses out and water diffuses in, PMMA forms a porous material, and is brittle. However, the hydrated PAAc polymers trapped in the PMMA-rich phase make the nanocomposite ductile.

The self-assembly process is applicable to other combinations of polymers. For example, we synthesize a nanocomposite of cellulose acetate and PAAc, of poly(ethyl methacrylate) and PAAc, and of PMMA–poly(N,N-dimethylacrylamide) (*SI Appendix*, Fig. S9). In all cases, the water content is over 40%, the elastic modulus is over 190 MPa, the strength is over 8 MPa, and the toughness is over 2,500 J·m^{-2} (*SI Appendix*, Table S5).

Conclusion

In summary, we have demonstrated nanocomposites that achieve attributes resembling load-bearing biological tissues: high water content and excellent mechanical properties. We fabricate the

nanocomposite through a self-assembly process, and demonstrate the generality of this process with widely used polymer glasses and hydrogel precursors. The rubbery stage during the process enables the fabrication of objects of complex shapes and fine features. The nanocomposites are homogeneous above the nanoscale phase size, resulting in high fidelity during nanofabrication. The nanocomposites may find applications in which water permeability and load-bearing capacity are both important. Examples include artificial tissues, high-pressure filters, low-friction coatings, and solid electrolytes. Furthermore, the process is generally applicable for natural and synthetic polymers. This self-assembling process opens doors to combine extremely different polymers to achieve unusual properties.

Materials and Methods

Synthesis of the PMMA–Water–PAAc Nanocomposites. Acrylic films (McMaster-Carr 8560K172), thickness ∼1.56 mm, were used as purchased. Acrylic acid (AAc, 147230), N,N′-methylenebisacrylamide (MBAA, M7279), and 2-hydroxy-4′-(2-hydroxyethoxy)-2-methylpropiophenone (Irgacure 2959, 410896) were purchased from Sigma Aldrich and used as received. Deionized water was purchased from Poland Spring. The water–AAc binary solution was prepared by mixing water, AAc, MBAA, and Irgacure 2959 with a fixed MBAA–AAc molar ratio of 0.001 and Irgacure 2959–AAc molar ratio of 0.001, but different water–AAc molar ratios W ranging from 0 to 14. Specifically, for the water–AAc binary solution of $W = 4$, 450 g of AAc, 450 g of water, 0.963 g of MBAA, and 1.4 g of Irgacure 2959 were added in a polyethylene bottle (McMaster-Carr, 41055T26), and heated in a 65 °C oven for 1 h to facilitate the dissolution of MBAA and Irgacure 2959. After heating, the bottle was gently shaken by hand for 1 min. For all values of W, the water–AAc binary solutions obtained were clear and transparent. Then 300 mL of the water–AAc binary solution was poured into a polypropylene storage container (McMaster-Carr, 6840A3), and an 80 mm × 80 mm PMMA film was immersed in the solution. The container was sealed by the lid, and stored in an oven at $T_{II} = 25$ °C or 65 °C, and was kept in darkness. The PMMA film was weighed every day, and the PMMA–water–AAc phase (stage II) was obtained when the weight reached a plateau. The PMMA–water–AAc phase was taken out from the container, wiped with tissues, held between two glass slides, and put into a polyethylene zip bag (VWR, 4662002). The bag was pressed to get rid of the air in it, zipped, and irradiated with UV light (15 W 365 nm, UVP XX-15L) for 6 h. For T_{III} higher than room temperature, the sample was cured on a hot plate. Upon UV polymerization, the PMMA–water–AAc phase turned into a PMMA–water–PAAc nanocomposite. During the step from stage II to stage III, the sample was held between two glass slides and sealed in a plastic bag, so that evaporation was negligible. The obtained nanocomposite was immersed in pure water at T_{IV} to swell to equilibrium. After that, all the samples were stored in water at 25 °C before testing.

Synthesis of the Cellulose Acetate–Water–PAAc Nanocomposites. Cellulose acetate film (8564K48) was purchased from McMaster-Carr. The cellulose acetate film and a water–AAc binary solution of $W = 6$ were used in the preparation, T_{II} was fixed at 25 °C, T_{III} was fixed at 25 °C, and T_{IV} was fixed at 65 °C. Otherwise, the preparation procedures were the same as the preparation of the PMMA–water–PAAc nanocomposites.

Synthesis of the Poly(ethyl Methacrylate)–Water–PAAc Nanocomposites. Poly(ethyl methacrylate) was first prepared. Thirty grams of ethyl methacrylate (Sigma Aldrich, 234893) and 0.005 g of 2,2′-Azobis(2-methylpropionitrile) (Sigma Aldrich, 441090) were mixed, and were cured in a mold at 65 °C for 12 h to get a poly(ethyl methacrylate) film with a thickness of ∼0.8 mm. The poly(ethyl methacrylate) film and a water–AAc binary solution of $W = 4$ were used in the preparation. T_{II} was fixed at 25 °C, T_{III} was fixed at 25 °C, and T_{IV} was fixed at 65 °C. Otherwise, the preparation procedures were the same as the preparation of the PMMA–water–PAAc nanocomposites.

Synthesis of the PMMA–Water–Poly(N,N-dimethylacrylamide) Nanocomposites. N,N-dimethylacrylamide (DMA, 274135) was purchased from Sigma Aldrich, and used as received. The water–DMA binary solution was prepared by mixing water, AAc, DMA, and Irgacure 2959 with a fixed water–DMA molar ratio of 1.2, MBAA–DMA molar ratio of 0.001, and Irgacure 2959–DMA molar ratio of 0.001. Specifically, 300 g of DMA, 65.5 g of water, 0.467 g of MBAA, and 0.679 g of Irgacure 2959 were added in an HDPE bottle (McMaster-Carr, 41055T26), and heated in a 65 °C oven for 1 h to facilitate the dissolution of MBAA and Irgacure 2959. The water–DMA binary solution was used in the preparation, T_{II} was fixed at 25 °C, T_{III} was fixed at 25 °C, and T_{IV} was fixed at 65 °C. Otherwise, the preparation procedures were the same as the preparation of the PMMA–water–PAAc nanocomposites.

Measurements of Stress–Stretch Curves for the PMMA–Water–AAc Phase. The test samples were cut into a dumbbell shape by a die cutter (Ace steel rule dies, ISO 527-2-5B), and tested by Instron 5966 with a 100-N load cell. During stretching, the force F and the displacement L_D were recorded. The gauge length was fixed to 21 mm and regarded as the sample's initial length (L_1). The samples were stretched monotonically until rupture, and the stretch rate was fixed at 0.01 s^{-1} unless otherwise noted. The stress was calculated by force divided by the cross-sectional area of the undeformed sample, and the stretch was calculated by $1 + L_D/L_1$. The elastic modulus was obtained from the slope of the stress–stretch curve in the linear elastic region (stretch < 1.05). For the stress relaxation tests, the PMMA–water–AAc phase of $W = 4$ was first coated with a layer of mineral oil (330779, Sigma Aldrich) to prevent evaporation. The sample was loaded on the Instron machine and pulled to a constant stretch of two at a rate of 0.1. The stretch was maintained for 30 min, and the force was recorded.

Measurements of Stress–Stretch Curves for the PMMA–Water–PAAc Nanocomposite and Pristine PMMA. Samples were cut by using a laser cutter (Helix 75 W, Epilog Laser), and tested by Instron 5966 with a 10-kN load cell. During stretching, the force F and the displacement L_D were recorded. Dumbbell-shaped samples (ISO 527-2-5B) were used to get the stress–stretch curves and strength. The samples were stretched monotonically to break, and the stretch rate was fixed at 0.01 s^{-1}. The strength was obtained by the maximum stress in the stress–stretch curves. The elastic modulus was obtained by testing a sample of rectangular shapes (width 5 mm, length 50 mm). The sample was preloaded with ∼8 N, and stretched monotonically to a stretch of 1.05.

Measurement of Toughness and Fatigue Resistance of PMMA–Water–PAAc Nanocomposite and Pristine PMMA. The toughness was obtained from a single-edge crack test. The sample was first cut using the laser cutter into a rectangular shape (width 20 mm, length 60 mm) with a 5-mm edge crack in the middle of the long side. The sample was loaded on the Instron with a gauge length of ∼45 mm. The stress, σ, is calculated by the force, F, divided by the uncut cross-sectional area. The energy release rate G is given by

$$G = \pi\sigma^2 a/E[1.122 - 0.231(a/b) + 10.55(a/b)^2 - 21.71(a/b)^3 + 30.382(a/b)^4]^2,$$

where a is the crack length, b is the width of the sample, and E is the elastic modulus (35). When the sample broke, the stress recorded was used to determine the toughness G_c.

Fatigue Tests. The fatigue test was performed by applying cyclic loading to a sample with a single-edge crack. The sample was first cut using the laser cutter into a rectangular shape (width 20 mm, length 60 mm). A precut crack of length ∼6 mm was introduced to the sample in the middle of the long side using a razor blade. The sample was stretched until the force reached the prescribed value, and unloaded with the same rate until the force reached zero. For every sample, the loading–unloading cycle was repeated for at least 5,000 cycles. To avoid dehydration, all tests were conducted in a humidity chamber, where the relative humidity was set to be ∼95%. Samples were weighed before and after testing, and the mass change was less than 2%. By varying the force in each test, the crack extension was measured for different values of G. The crack extension, dc, was measured using an optical microscope. The crack extension was divided by the number of cycles, dN, and plotted against different values of G. The frequency of cyclic loading was fixed for all tests at 0.1 Hz.

Scanning Electron Microscope. The images were conducted using a scanning electron microscope (Zeiss Ultra Plus FESEM). All the samples were freeze-dried for 3 d before tests. For characterization of the phase size, all the samples were first immersed in liquid nitrogen for 1 min, and then broken to expose the cross-section.

The cross-section was then coated with a 5-nm-thick Pt/Pd layer using a metal sputter (208HR, Cressington Scientific Instruments), and proceeded to the imaging.

Data Availability. All study data are included in the article and/or supporting information.

ACKNOWLEDGMENTS. This work was supported by the Harvard University Materials Research Science and Engineering Center (Grant DMR-2011754). We acknowledge the support of the Air Force Office of Scientific Research under award number FA9550-20-1-0397. J.K. acknowledges financial support from the Kwanjeong Educational Foundation.

Author affiliations: [a]John A. Paulson School of Engineering and Applied Science, Harvard University, Cambridge, MA 02138

1. K. S. Koutroupi, J. C. Barbenel, Mechanical and failure behaviour of the stratum corneum. *J. Biomech.* **23**, 281–287 (1990).
2. I. H. Blank, Factors which influence the water content of the stratum corneum. *J. Invest. Dermatol.* **18**, 433–440 (1952).
3. K. S. Wu, W. W. van Osdol, R. H. Dauskardt, Mechanical properties of human stratum corneum: Effects of temperature, hydration, and chemical treatment. *Biomaterials* **27**, 785–795 (2006).
4. J.-Y. Sun *et al.*, Highly stretchable and tough hydrogels. *Nature* **489**, 133–136 (2012).
5. A. Klein, P. G. Whitten, K. Resch, G. Pinter, Nanocomposite hydrogels: Fracture toughness and energy dissipation mechanisms. *J. Polym. Sci., B, Polym. Phys.* **53**, 1763–1773 (2015).
6. J. P. Gong, Why are double network hydrogels so tough? *Soft Matter* **6**, 2583 (2010).
7. T. Nakajima *et al.*, True chemical structure of double network hydrogels. *Macromolecules* **42**, 2184–2189 (2009).
8. T. L. Sun *et al.*, Physical hydrogels composed of polyampholytes demonstrate high toughness and viscoelasticity. *Nat. Mater.* **12**, 932–937 (2013).
9. J. Li, Z. Suo, J. J. Vlassak, Stiff, strong, and tough hydrogels with good chemical stability. *J. Mater. Chem. B Mater. Biol. Med.* **2**, 6708–6713 (2014).
10. X. Hu, M. Vatankhah-Varnoosfaderani, J. Zhou, Q. Li, S. S. Sheiko, Weak hydrogen bonding enables hard, strong, tough, and elastic hydrogels. *Adv. Mater.* **27**, 6899–6905 (2015).
11. N. Rauner, M. Meuris, M. Zoric, J. C. Tiller, Enzymatic mineralization generates ultrastiff and tough hydrogels with tunable mechanics. *Nature* **543**, 407–410 (2017).
12. M. Hua *et al.*, Strong tough hydrogels via the synergy of freeze-casting and salting out. *Nature* **590**, 594–599 (2021).
13. C. Liu *et al.*, Tough hydrogels with rapid self-reinforcement. *Science* **372**, 1078–1081 (2021).
14. J. Kim, G. Zhang, M. Shi, Z. Suo, Fracture, fatigue, and friction of polymers in which entanglements greatly outnumber cross-links. *Science* **374**, 212–216 (2021).
15. D. R. King *et al.*, Extremely tough composites from fabric reinforced polyampholyte hydrogels. *Mater. Horiz.* **2**, 584–591 (2015).
16. Y. Huang *et al.*, Energy-dissipative matrices enable synergistic toughening in fiber reinforced soft composites. *Adv. Funct. Mater.* **27**, 1605350 (2017).
17. A. A. Barba, A. Dalmoro, F. De Santis, G. Lamberti, Synthesis and characterization of P(MMA-AA) copolymers for targeted oral drug delivery. *Polym. Bull.* **62**, 679–688 (2009).
18. S. S. Halacheva *et al.*, Injectable biocompatible and biodegradable pH-responsive hollow particle gels containing poly(acrylic acid): The effect of copolymer composition on gel properties. *Biomacromolecules* **15**, 1814–1827 (2014).
19. A. Abusafieh, R. Gobran, S. R. Kalidindi, Synthesis and characterization of a poly(methyl methacrylate-acrylic acid) copolymer for bioimplant applications. *J. Appl. Polym. Sci.* **63**, 75–87 (1997).
20. D. Das, E. Cha, S. Lee, H. Shin, I. Noh, Effects of molar ratios of two immiscible monomers toward development of an amphiphilic, highly stretchable, bioadhesive, self-healing copolymeric hydrogel and its mineral-active cellular behavior. *Biomacromolecules* **21**, 892–902 (2020).
21. U. Ali, K. J. Bt. A. Karim, N. A. Buang, A review of the properties and applications of poly (methyl methacrylate) (PMMA). *Polym. Rev. (Phila. Pa.)* **55**, 678–705 (2015).
22. H. Cho *et al.*, Replication of flexible polymer membranes with geometry-controllable nano-apertures via a hierarchical mould-based dewetting. *Nat. Commun.* **5**, 3137 (2014).
23. I. D. Johnston, D. K. McCluskey, C. K. L. Tan, M. C. Tracey, Mechanical characterization of bulk Sylgard 184 for microfluidics and microengineering. *J. Micromech. Microeng.* **24**, 035017 (2014).
24. K. D. Ziegel, A. Romanov, Modulus reinforcement in elastomer composites. I. Inorganic fillers. *J. Appl. Polym. Sci.* **17**, 1119–1131 (1973).
25. J. Wang, L. Lin, Q. Cheng, L. Jiang, A strong bio-inspired layered PNIPAM-clay nanocomposite hydrogel. *Angew. Chem. Int. Ed. Engl.* **51**, 4676–4680 (2012).
26. T. R. Clark, R. W. Hertzberg, N. Mohammadi, Fatigue mechanisms in poly (methyl methacrylate) at threshold: Effects of molecular weight and mean stress. *J. Mater. Sci.* **28**, 5161–5168 (1993).
27. C. Fernández-Rico, T. Sai, A. Sicher, R. W. Style, E. R. Dufresne, Putting the squeeze on phase separation. *JACS Au* **2**, 66–73 (2021).
28. J. K. Yeo, L. H. Sperling, D. A. Thomas, Theoretical prediction of domain sizes in IPN's and related materials. *Polymer (Guildf.)* **24**, 307–313 (1983).
29. Y. Dong, D. C. Sundberg, Estimation of polymer/water interfacial tensions: Hydrophobic homopolymer/water interfaces. *J. Colloid Interface Sci.* **258**, 97–101 (2003).
30. P. J. Flory, *Principles of Polymer Chemistry* (Cornell University Press, 2006).
31. J. Li, Y. Hu, J. J. Vlassak, Z. Suo, Experimental determination of equations of state for ideal elastomeric gels. *Soft Matter* **8**, 8121 (2012).
32. A. P. Safronov, L. V. Adamova, A. S. Blokhina, I. A. Kamalov, P. A. Shabadrov, Flory-Huggins parameters for weakly crosslinked hydrogels of poly(acrylic acid) and poly(methacrylic acid) with various degrees of ionization. *Polym. Sci. Ser. A* **57**, 33–42 (2015).
33. J. Shen, C. C. Chen, J. A. Sauer, Effects of sorbed water on properties of low and high molecular weight PMMA: 1. Deformation and fracture behaviour. *Polymer (Guildf.)* **26**, 511–518 (1985).
34. I. M. Wienk *et al.*, Recent advances in the formation of phase inversion membranes made from amorphous or semi-crystalline polymers. *J. Membr. Sci.* **113**, 361–371 (1996).
35. H. Tada, P. C. Paris, G. R. Irwin, *The Stress Analysis of Cracks Handbook* (ASME Press, ed. 3, 2000).